eLIFE elifesciences.org

RESEARCH ARTICLE

Figures and figure supplements

Common activation mechanism of class A GPCRs

Qingtong Zhou *et al*

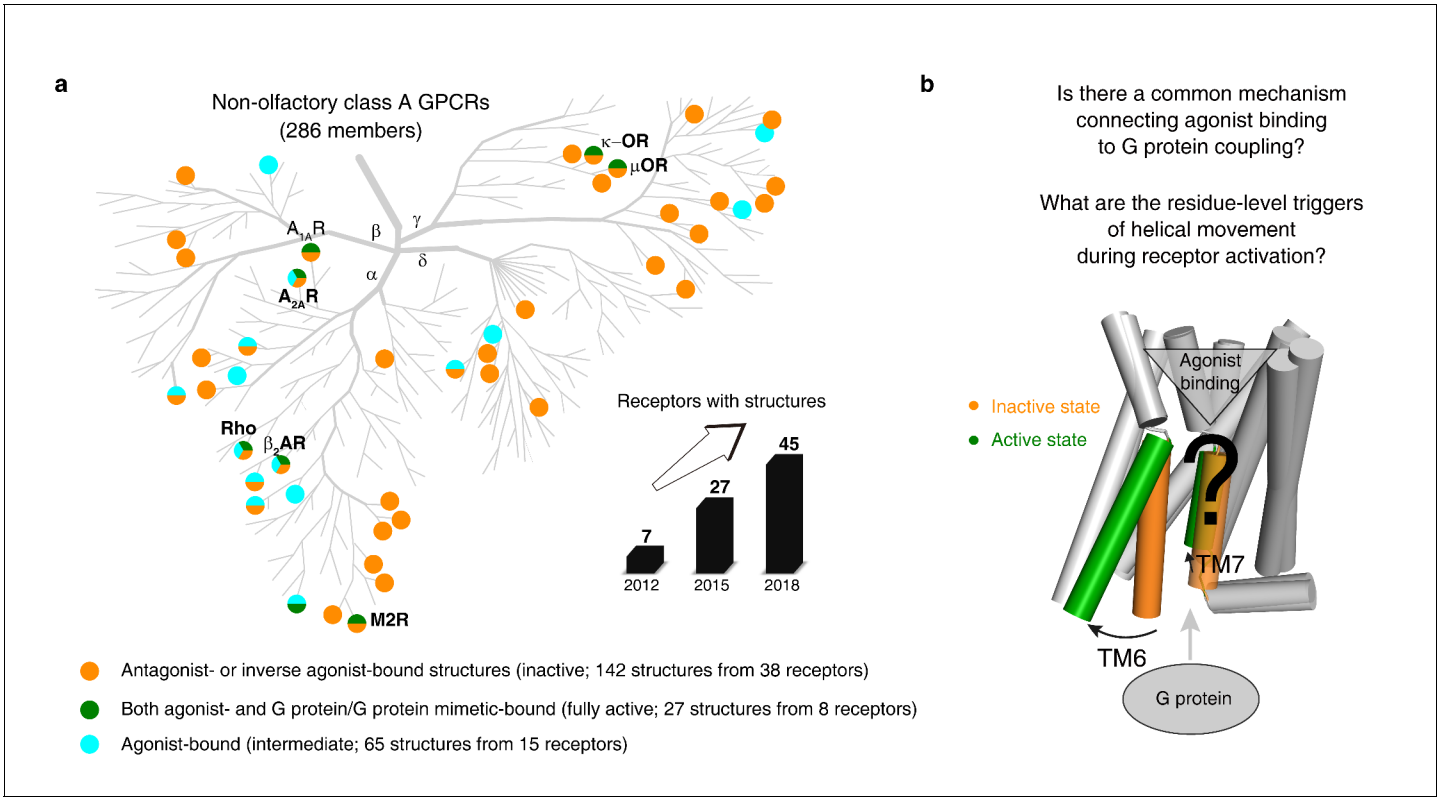

Figure 1. An increasing number of reported class A GPCR structures facilitates studies on common activation mechanism. (**a**) Distribution of structures in different states in the non-olfactory class A GPCR tree as of October 1, 2018. (**b**) Common GPCR activation mechanism and the residue-level triggers are not well understood.

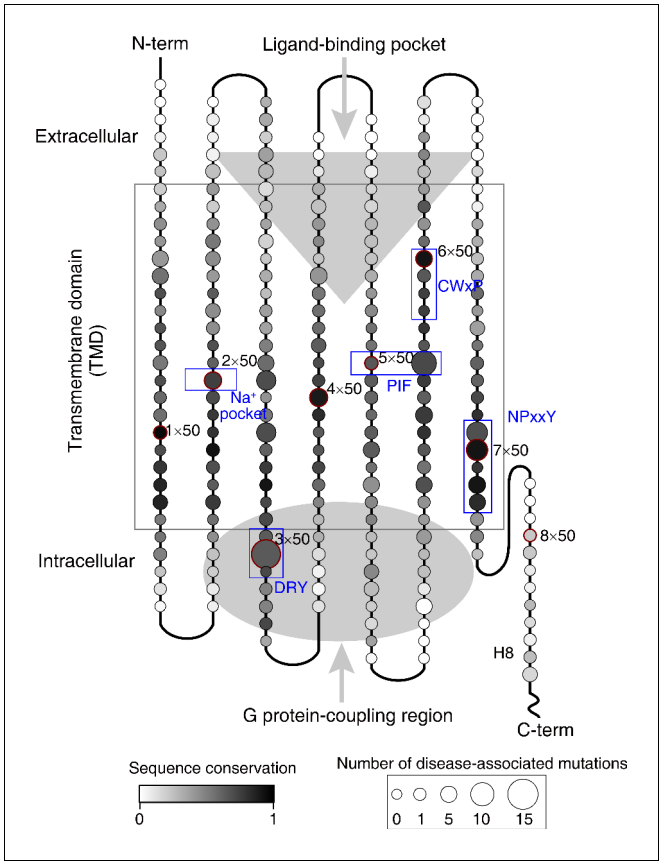

Figure 1—figure supplement 1. The pattern of conservation of residues and the map of number of disease-associated mutations in human class A GPCRs. The alignment of 286 non-olfactory, class A human GPCRs were obtained from the GPCRdb (***Hauser et al., 2018***; ***Isberg et al., 2016***; ***Pándy-Szekeres et al., 2018***; ***Isberg et al., 2015***) and sent for the sequence conservation score calculation for all residue positions by the Protein Residue Conservation Prediction (***Capra and Singh, 2007***) tool with scoring method 'Property Entropy" (***Mirny and Shakhnovich, 1999***). To obtain disease-associated mutations, we performed database integration and literature investigation for all 286 non-olfactory class A GPCRs. Four commonly used databases (UniProt [***The UniProt Consortium, 2017***], OMIM [***Amberger et al., 2011***], Ensembl [***Zerbino et al., 2018***] and GPCRdb) were first filtered by disease mutations and then merged. Finally, we collected 435 disease mutations from 61 class A GPCRs (***Figure 1—source data 2***).

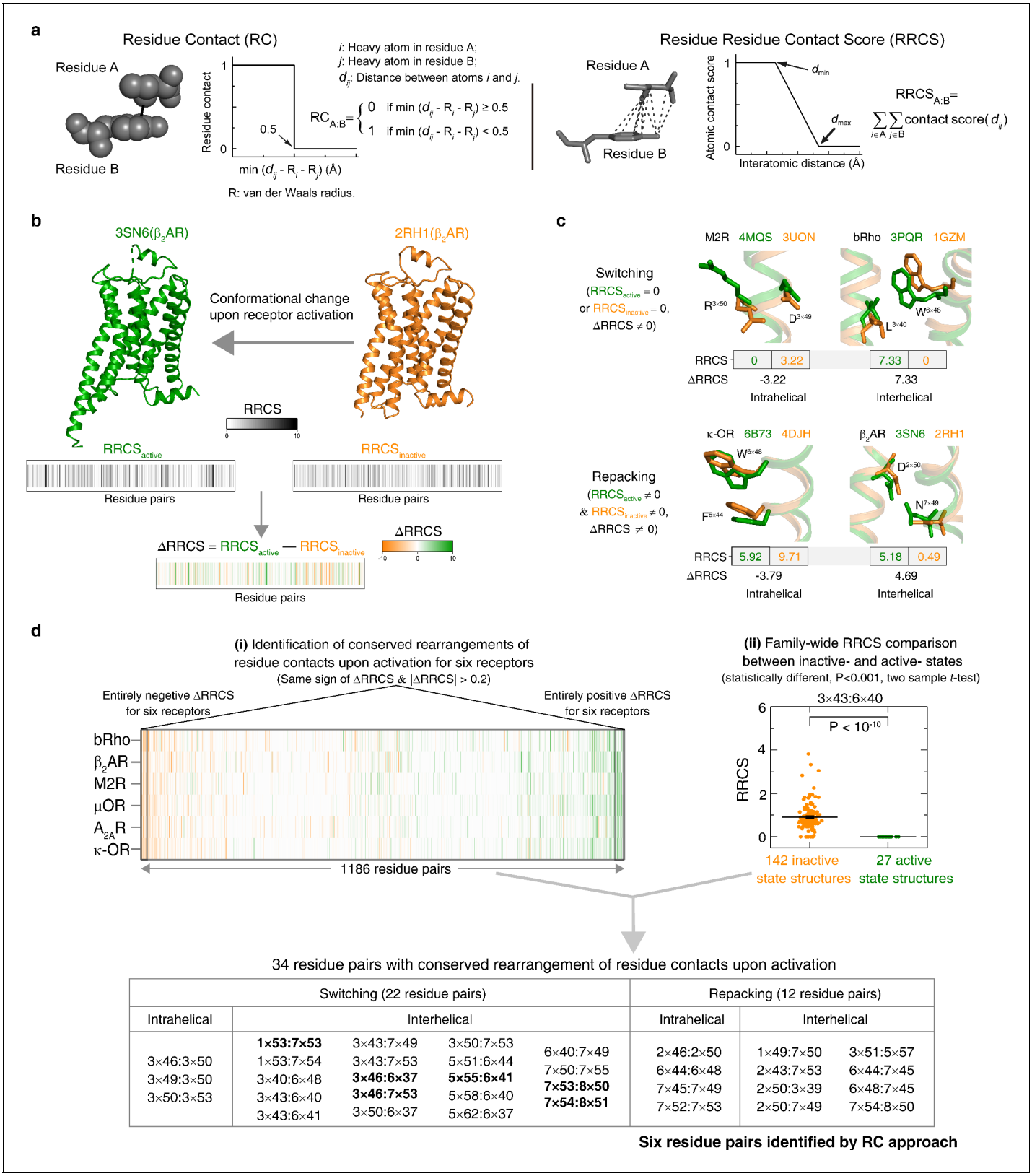

Switching (22 residue pairs)				Repacking (12 residue pairs)	
Intrahelical	Interhelical			Intrahelical	Interhelical
3×46:3×50	**1×53:7×53**	3×43:7×49	3×50:7×53	6×40:7×49	2×46:2×50	1×49:7×50	3×51:5×57
3×49:3×50	1×53:7×54	3×43:7×53	5×51:6×44	7×50:7×55	6×44:6×48	2×43:7×53	6×44:7×45
3×50:3×53	3×40:6×48	**3×46:6×37**	**5×55:6×41**	**7×53:8×50**	7×45:7×49	2×50:3×39	6×48:7×45
	3×43:6×40	**3×46:7×53**	5×58:6×40	**7×54:8×51**	7×52:7×53	2×50:7×49	7×54:8×50
	3×43:6×41	3×50:6×37	5×62:6×37				

Figure 2. Understanding GPCR activation mechanism by RRCS and ΔRRCS. (**a**) Comparison of residue contact (RC) (***Venkatakrishnan et al., 2016***) and residue residue contact score (RRCS) calculations. RRCS can describe the strength of residue-residue contact quantitatively in a much more accurate manner than the Boolean descriptor RC. (**b**) RRCS and ΔRRCS calculation for a pair of active and inactive structures can capture receptor

Figure 2 continued on next page

Figure 2 continued

conformational change upon activation. (**c**) Two types of conformational changes (i.e. switching and repacking contacts) can be defined by RRCS to quantify the global, local, major and subtle conformational changes in a systematic way. (**d**) Two criteria of identifying conserved residue rearrangements upon receptor activation by RRCS and ΔRRCS. Thirty-four residues pairs were identified based on the criteria (see Materials and methods, ***Figure 2—source datas 1*** and ***2*** for details), only six of them were discovered before (***Venkatakrishnan et al., 2016***).

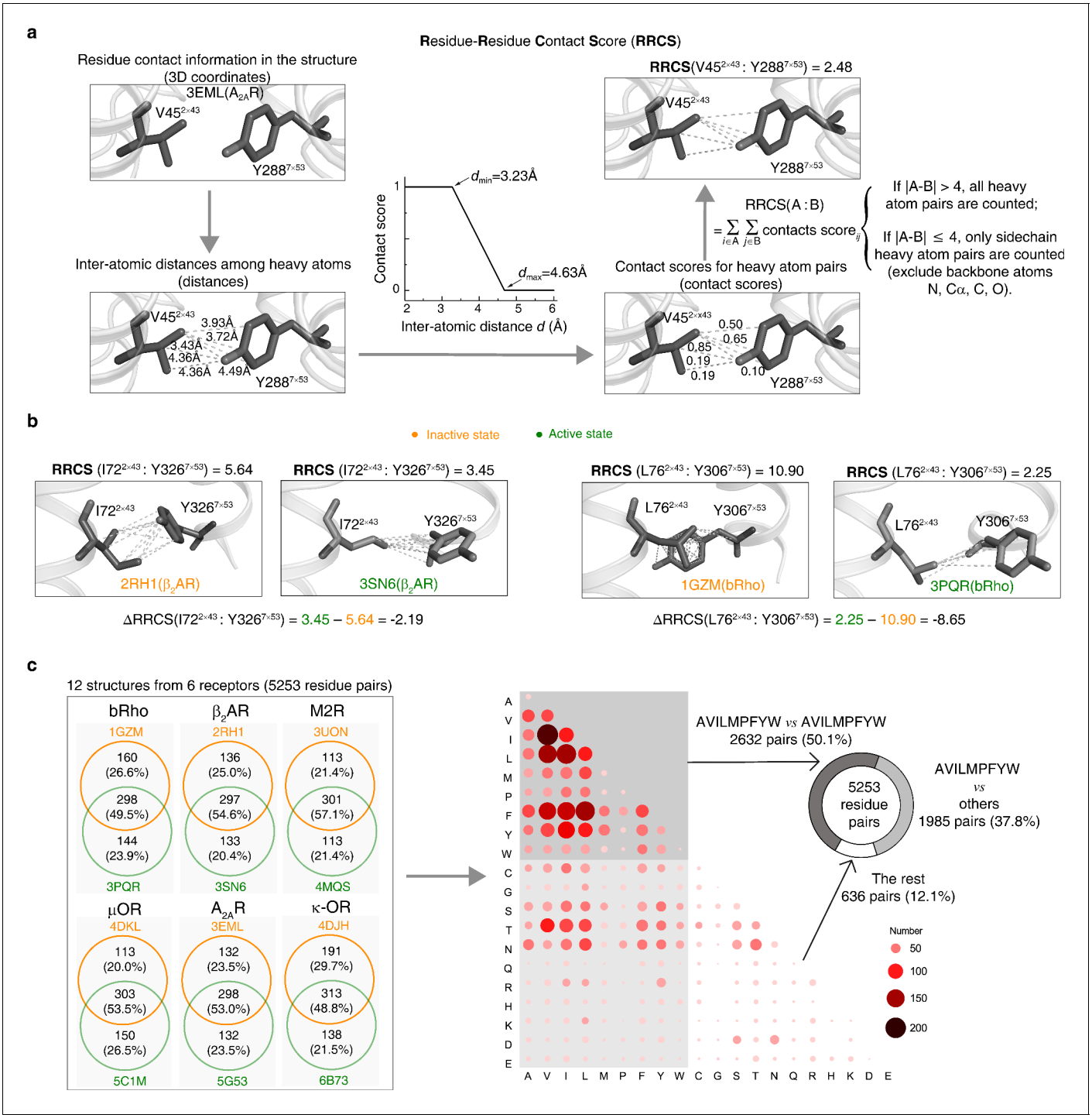

Figure 2—figure supplement 1. Calculation of RRCS and ΔRRCS. (**a**) Workflow of RRCS calculation. (**b**) Examples of RRCS and ΔRRCS calculation for two residues pairs. (**c**) Statistics of residue contacts and contact types for six receptors (bRho, β_2AR, M2R, μOR, A_{2A}R and κ-OR) in their inactive and active states. Contact type describes physicochemical properties of two interacted amino acids that form a pair. The amino acids with hydrophobic side chains (one-letter code: A, V, I, L, M, P, F, Y, W) contribute to the majority of residue contacts, either within themselves (50.1%) or with other amino acids (37.8%).

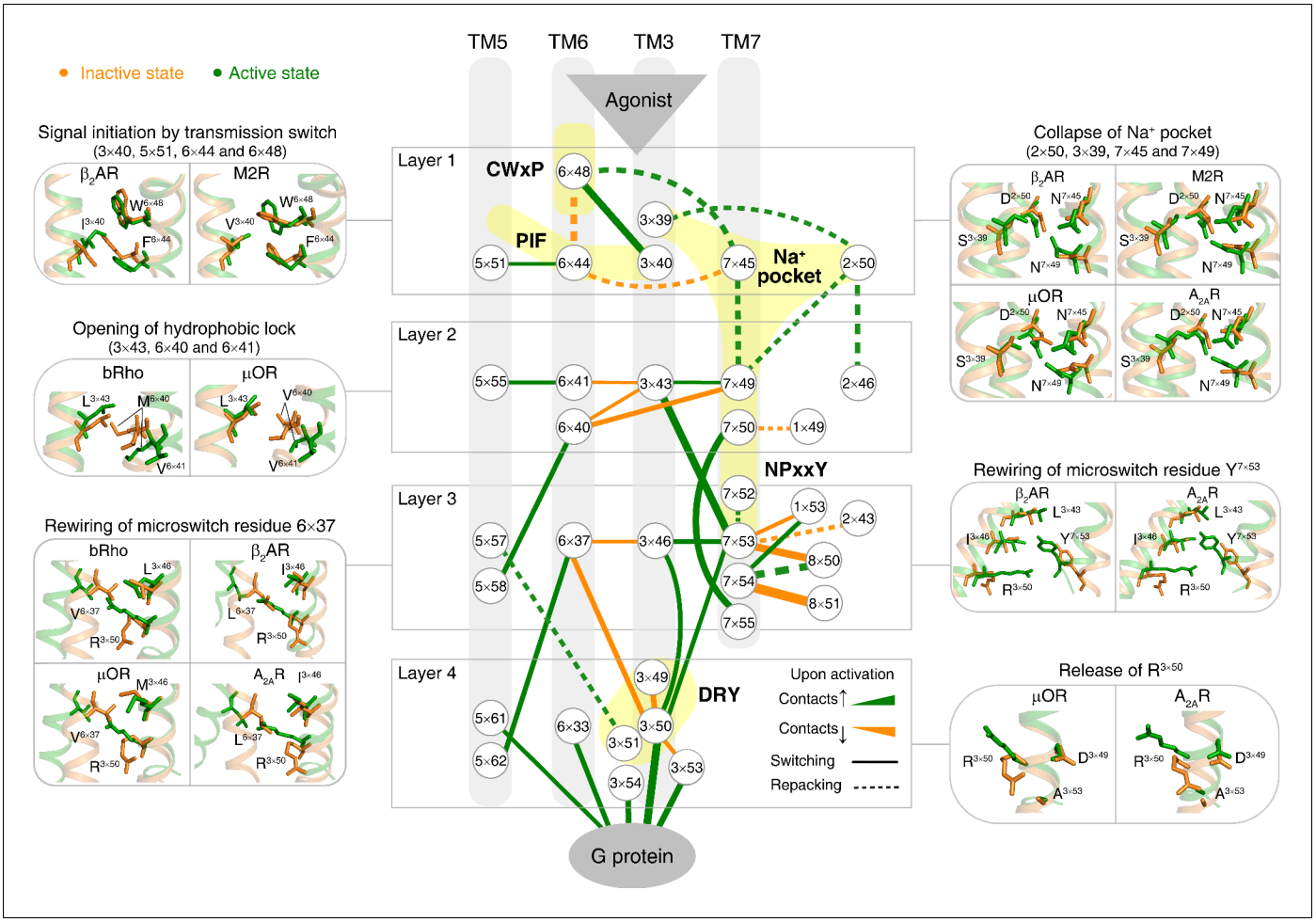

Figure 3. Common activation pathway of class A GPCRs. Node represents structurally equivalent residue with the GPCRdb numbering (***Isberg et al., 2016***) while the width of edge is proportional to the average ΔRRCS among six receptors (bRho, β_2AR, M2R, μOR, A_{2A}R and κ-OR). Four layers were qualitatively defined based on the topology of the pathway and their roles in activation: signal initiation (layer 1), signal propagation (layer 2), microswitches rewiring (layer 3) and G-protein coupling (layer 4).

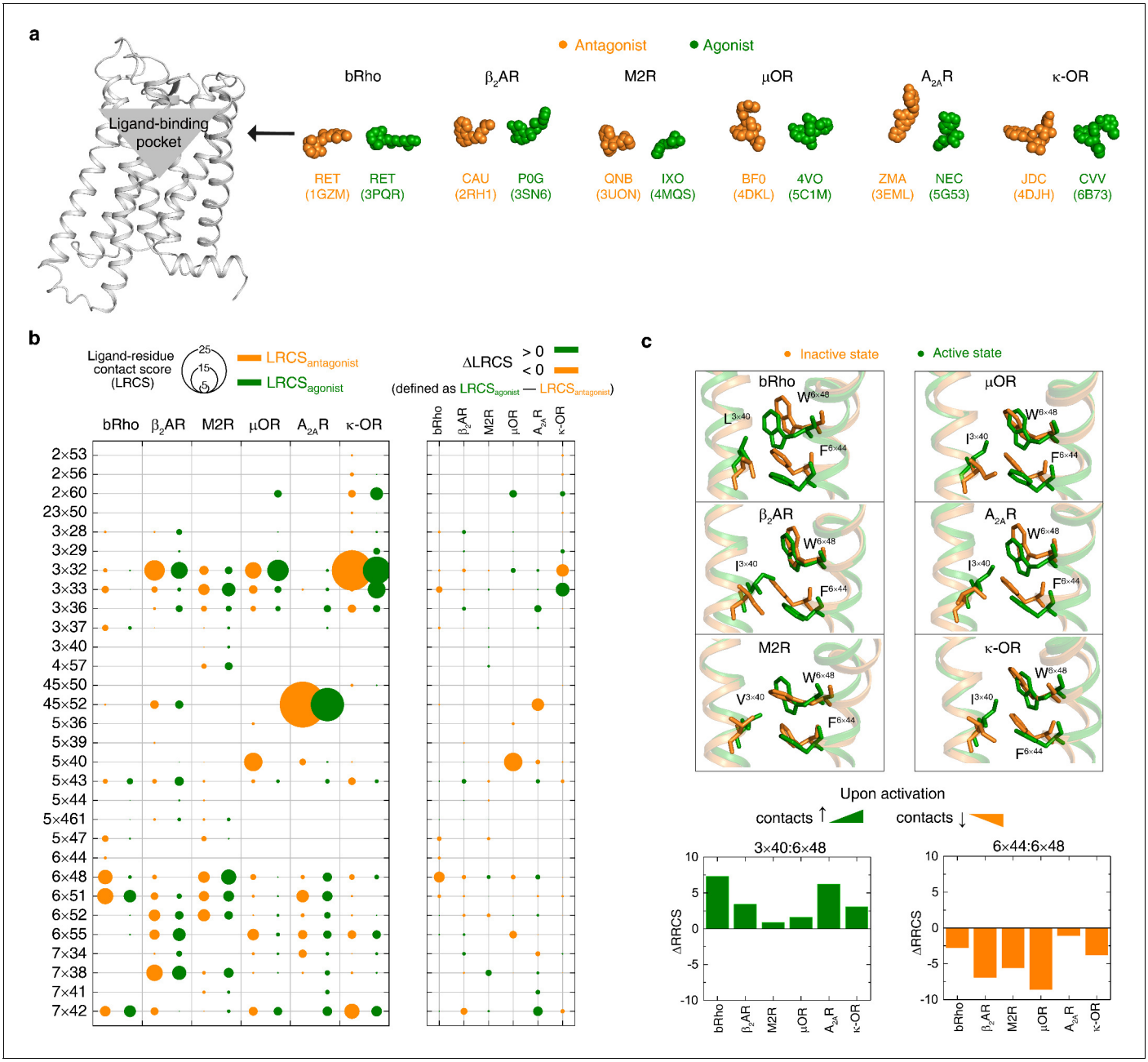

Figure 3—figure supplement 1. Rearrangements of ligand-residue contacts in ligand-binding pocket are not conserved, reflecting diverse ligand recognition modes. (**a**) Sphere representation of antagonist- and agonist-bound receptor crystal structures. (**b**) Diverse LRCS and ΔLRCS reveal the repertoire of ligand recognition across class A GPCRs. The agonist or antagonist was treated as a single residue when calculating LRCS and ΔLRCS. As shown by the calculated ΔRRCS, no ligand-residue pair exhibits conserved rearrangements upon activation. (**c**) Conserved conformational changes were only observed at the very bottom of ligand-binding pocket (6×48, 3×40 and 6×44).

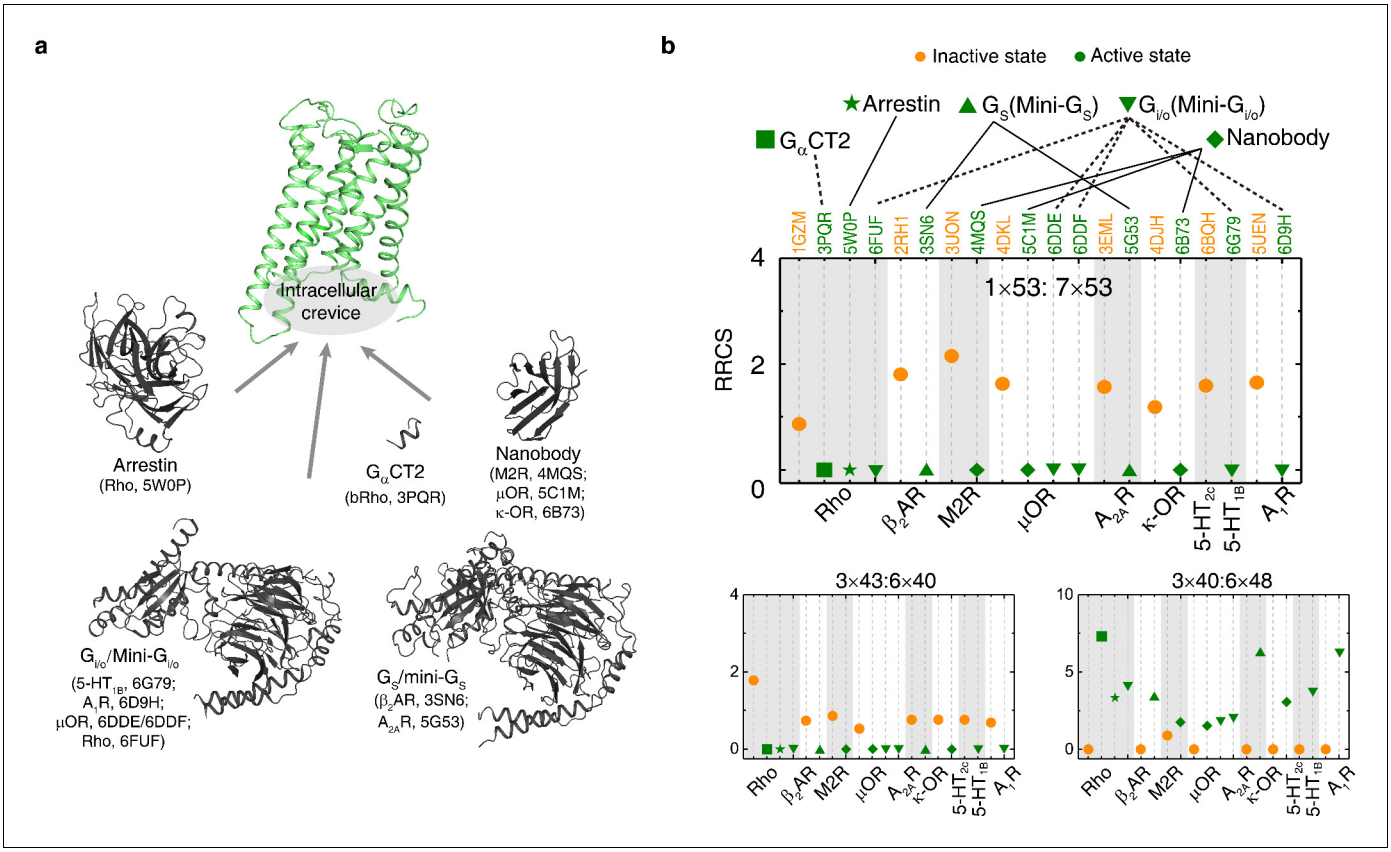

Figure 4. The common activation mechanism is the shared portion of various downstream pathways of different class A GPCRs. (**a**) Intracellular binding partners used in the active state structures. (**b**) Comparison of RRCS for active (green) and inactive (orange) states of eight receptors with different intracellular binding partners, including four recently solved cryo-EM structures of $G_{i/o}$-bound receptors (5-HT_{1B} receptor, rhodopsin, A_1R and μOR) (***Tsai et al., 2018***; ***García-Nafría et al., 2018***; ***Kang et al., 2018***; ***Koehl et al., 2018***; ***Draper-Joyce et al., 2018***) whose resolutions were low (usually ≥3.8 Å for the GPCR part). Nevertheless, almost all conserved residue rearrangements in the pathway can be observed from them. Three of 34 residues pairs were shown here, see ***Figure 4—figure supplements 1*** and ***2*** for the remaining 31 residue pairs.

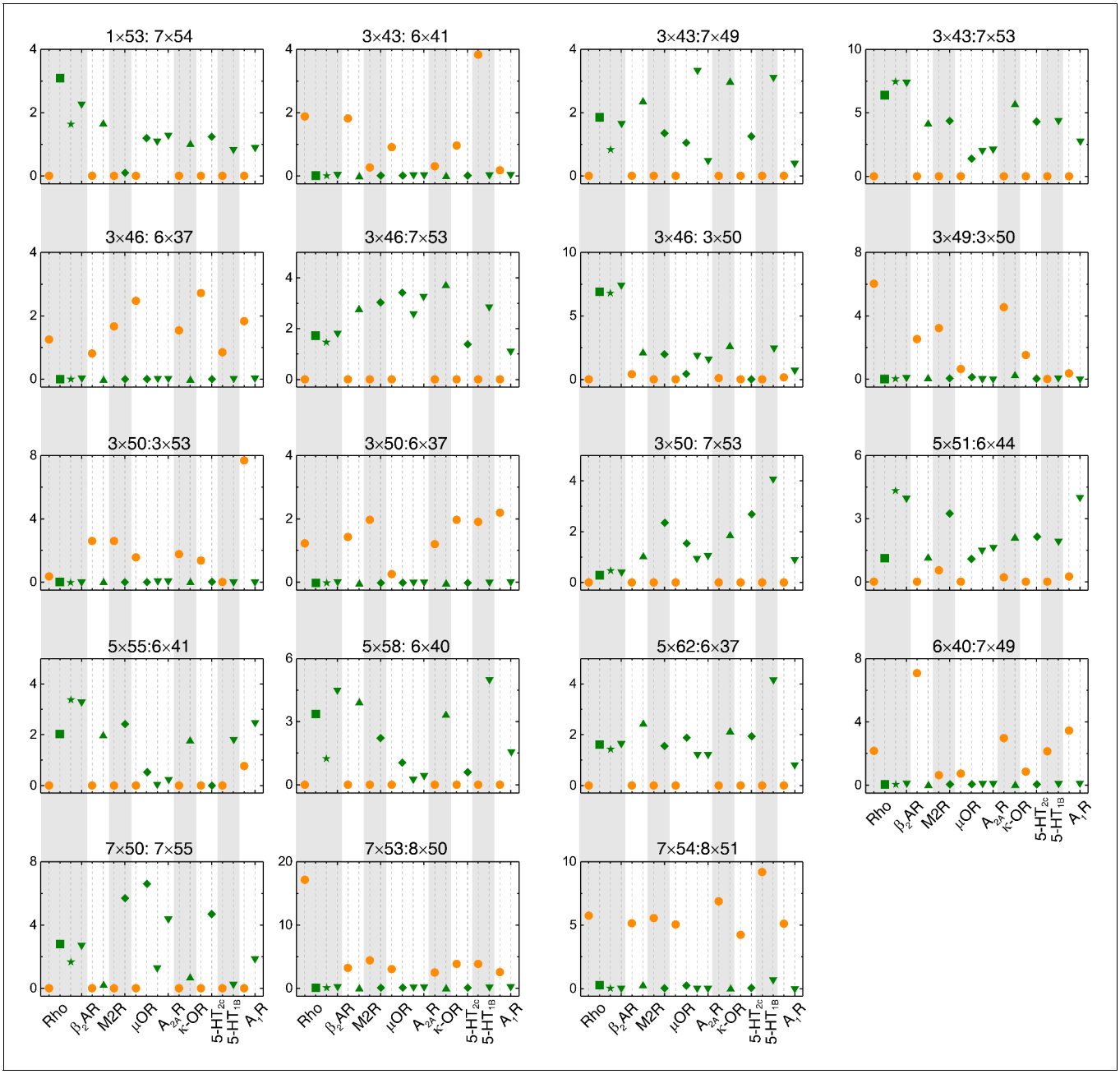

Figure 4—figure supplement 1. The switching conformation change is conserved upon receptor activation. Comparison of RRCS for active (green) and inactive (orange) states of eight receptors with different intracellular binding partners, including four recently solved cryo-EM structures of $G_{i/o}$-bound receptors (5-HT_{1B} receptor, rhodopsin, A_1R and μOR) whose resolutions were low (usually ≥3.8 Å for the GPCR part). Nevertheless, almost all conserved residue rearrangements in the pathway can be observed from them. Nineteen of 34 residues pairs were shown here, see ***Figure 4*** and ***Figure 4—figure supplement 2*** for the remaining residue pairs.

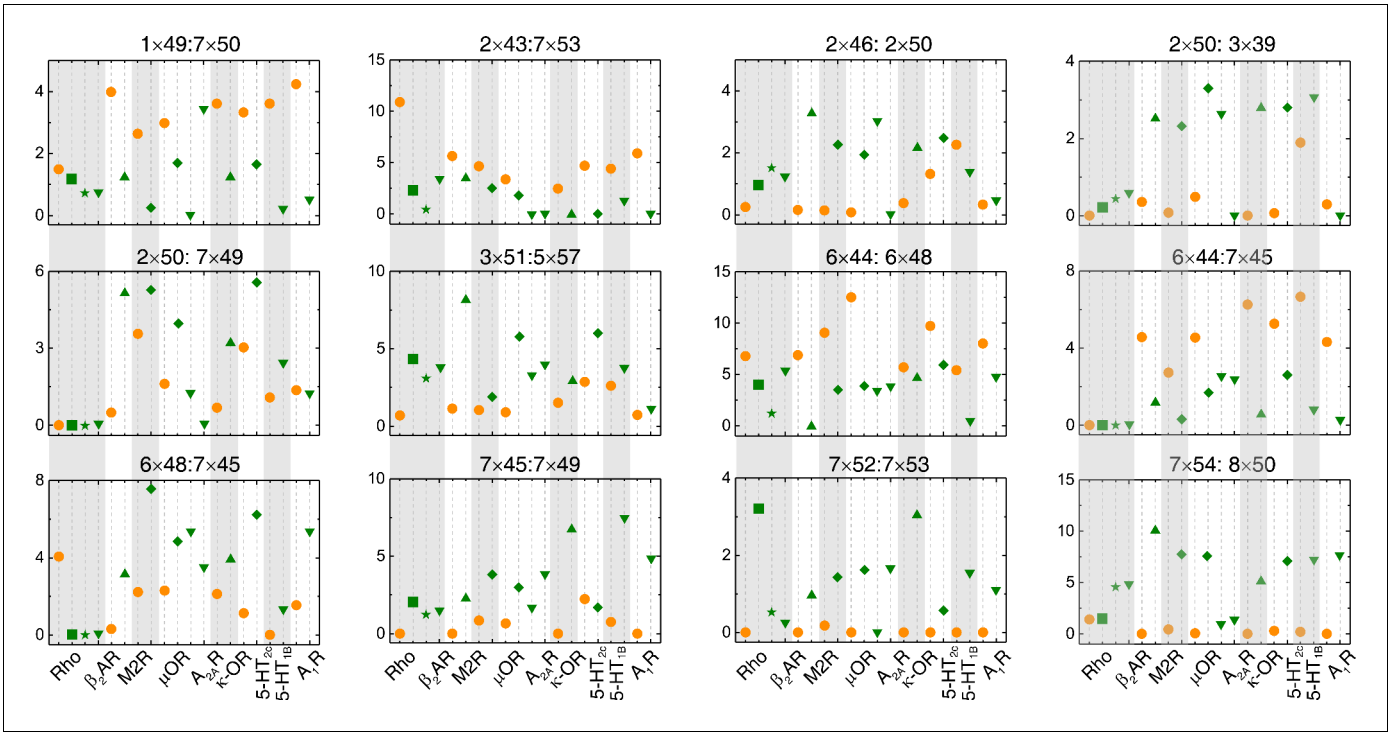

Figure 4—figure supplement 2. The repacking conformation change is conserved upon receptor activation. Comparison of RRCS for active (green) and inactive (orange) states of eight receptors with different intracellular binding partners, including four recently solved cryo-EM structures of $G_{i/o}$-bound receptors (5-HT_{1B} receptor, rhodopsin, A_1R and μOR) whose resolutions were low (usually ≥3.8 Å for the GPCR part). Nevertheless, almost all conserved residue rearrangements in the pathway can be observed from them. Twelve of 34 residues pairs were shown here, see ***Figure 4*** and ***Figure 4—figure supplement 1*** for the remaining residue pairs.

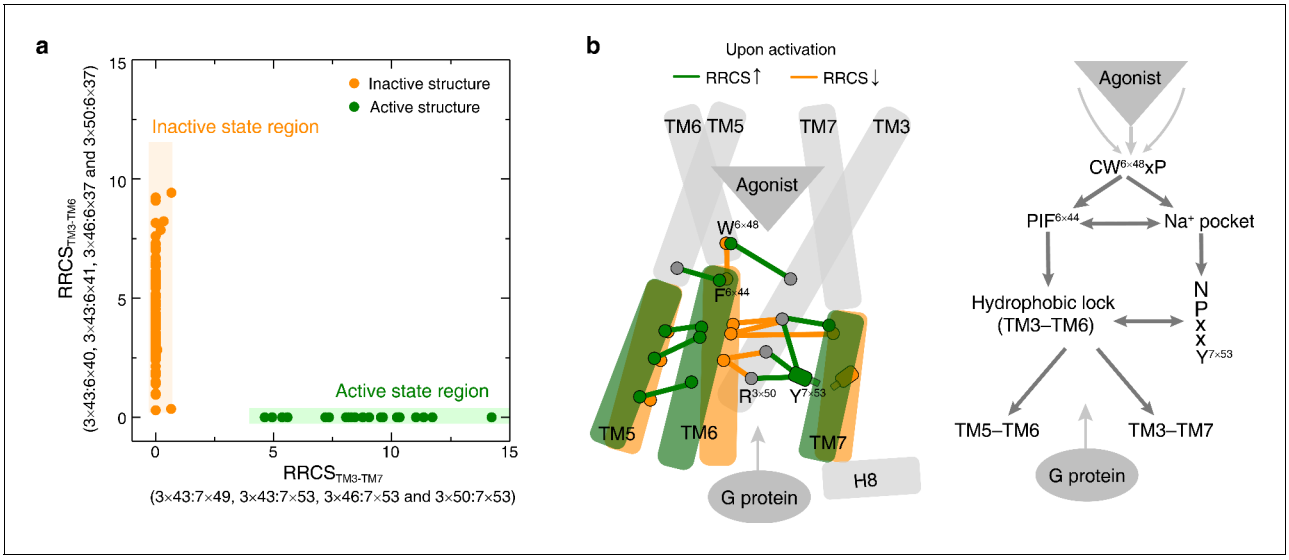

Figure 5. Common activation model of class A GPCRs reveals major changes upon GPCR activation. (**a**) Active and inactive state structures form compact clusters in the 2D inter-helical contact space: $RRCS_{TM3-TM7}$ (X-axis) and $RRCS_{TM3-TM6}$ (Y-axis). GPCR activation is best described by the outward movement of TM6 and inward movement of TM7, resulting in switch in the contacts of TM3 from TM6 to TM7. (**b**) Common activation model for class A GPCRs. Residues are shown in circles, conserved contact rearrangements of residue pairs upon activation are denoted by lines.

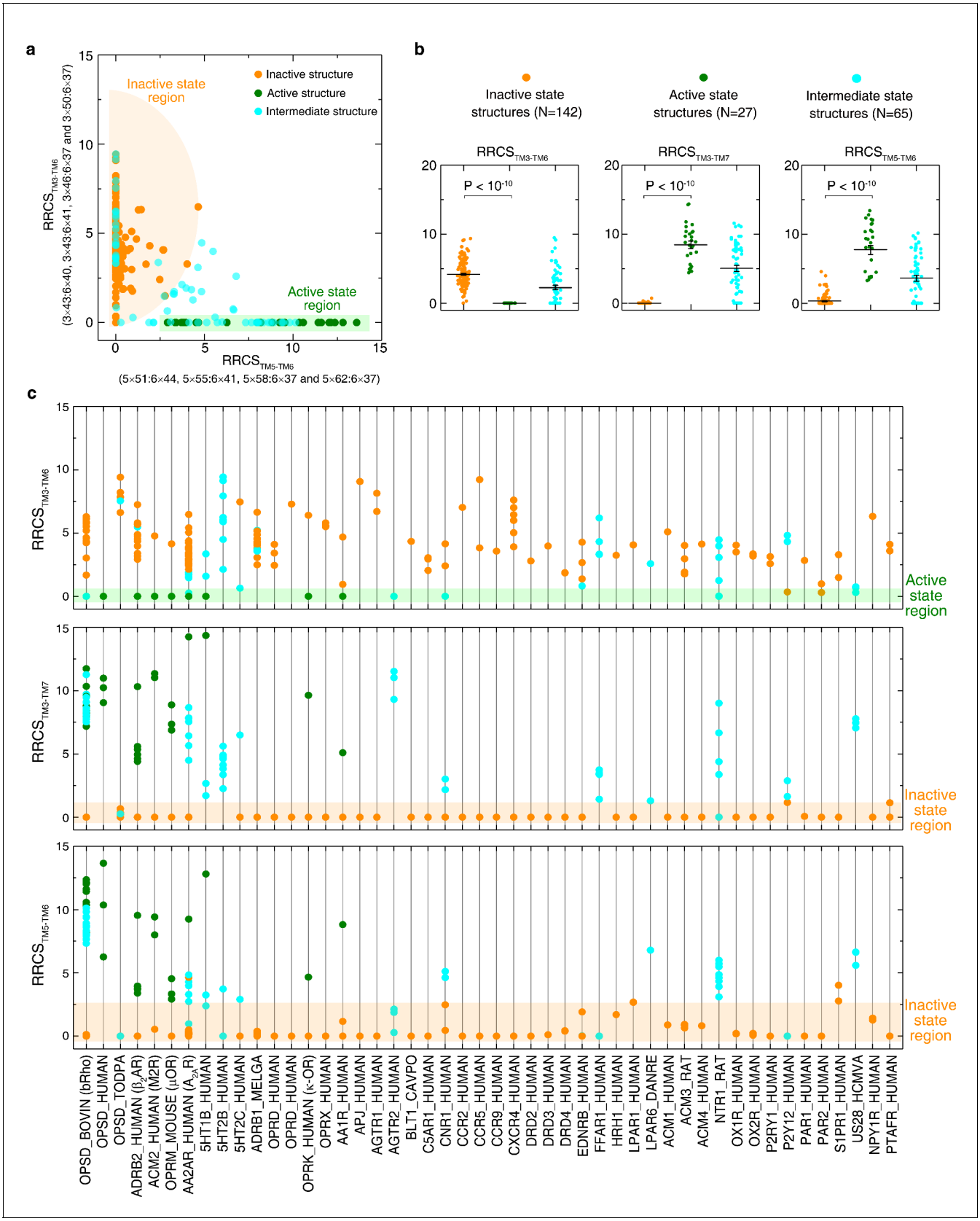

Figure 5—figure supplement 1. Global conformational change upon activation. (**a**) Distinct clustering of inactive- and active-state structures in two-dimentional inter-helical contact space $RRCS_{TM5\text{-}TM6}$ *vs.* $RRCS_{TM3\text{-}TM6}$. (**b**) The inter-helical contacts comparison between inactive- and active-state

Figure 5—figure supplement 1 continued on next page

Figure 5—figure supplement 1 continued

structures. (**c**) Receptor-specific inter-helical contacts for all class A GPCR structures (inactive, intermediate and active states are colored in orange, cyan and green, respectively). These results demonstrate that receptor activation involves the elimination of TM3-TM6 contacts, formation of TM3-TM7 and TM5-TM6 contacts, reflecting the outward movement of the cytoplasmic end of TM6 away from TM3, the inward movement of TM7 towards TM3 and the repacking of TM5 and TM6.

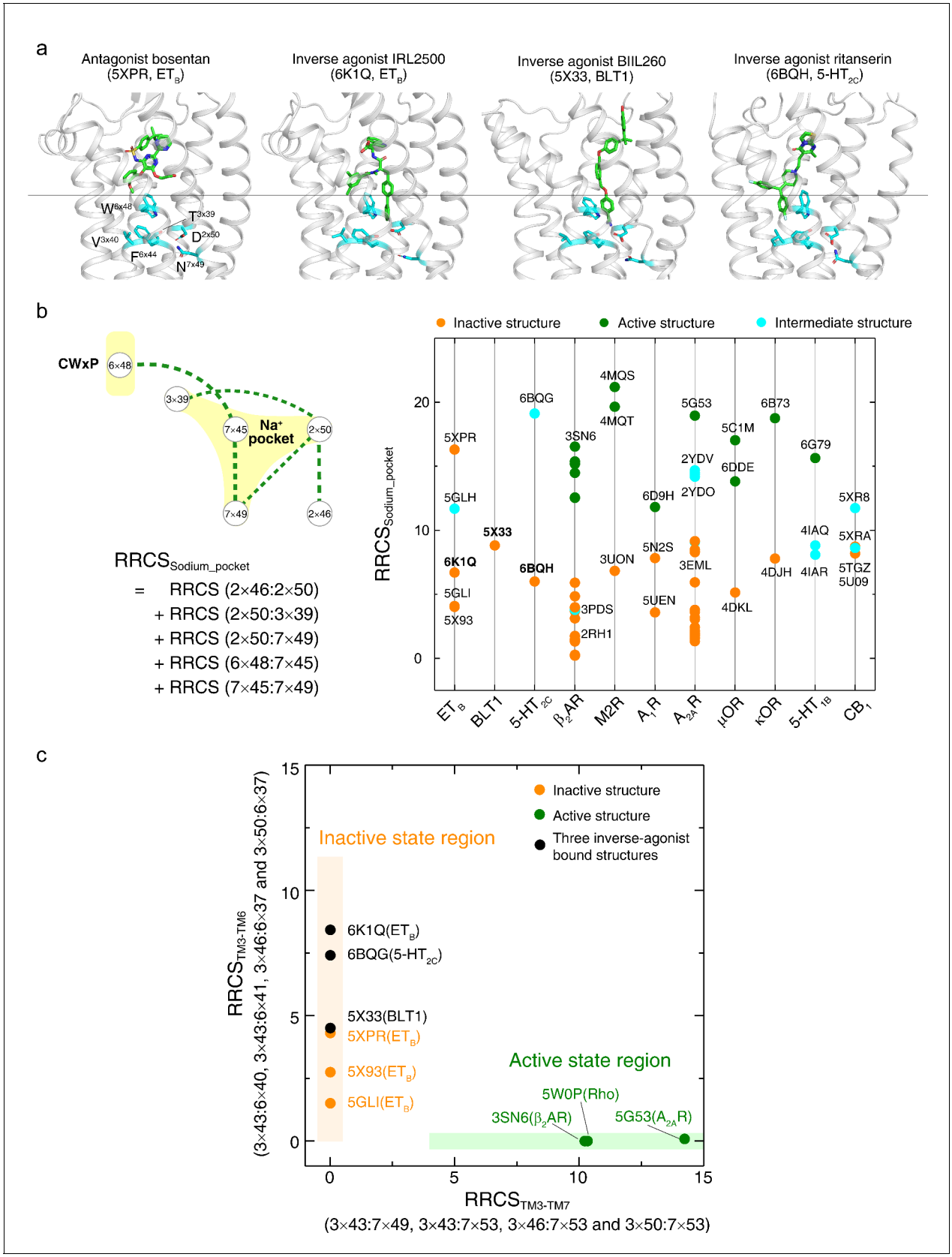

Figure 5—figure supplement 2. An inverse-agonism of class A GPCRs by preventing the collapse of Na^+ pocket. (**a**) Comparison of binding poses of antagonist (bosentan [***Shihoya et al., 2017***]) and inverse agonists (IRL2500 [***Nagiri et al., 2019***], BIIL260 [***Hori et al., 2018***] and ritanserin [***Peng et al.,***

Figure 5—figure supplement 2 continued on next page

Figure 5—figure supplement 2 continued

2018]). Inverse agonists diffuse deeper in the ligand-binding pocket to touch the Na^+ pocket. These key residues around the Na^+ pocket are shown. (**b**) Comparison of the sum of contact scores of the conserved residue pairs around the Na^+ pocket ($RRCS_{sodium\_pocket}$) between inactive- and active-state structures. The collapse of the Na^+ pocket leads to a denser repacking of six residues (five residue pairs), reflected by higher $RRCS_{sodium\_pocket}$ scores compared to that of the inactive state structures. (**c**) Distribution of three inverse agonist bound structures in the 2D inter-helical contact space: $RRCS_{TM3\text{-}TM7}$ (X-axis) and $RRCS_{TM3\text{-}TM6}$ (Y-axis). These inverse agonists bound structures (5×33, 6BQG and 6K1Q) located in the inactive state region with zero $RRCS_{TM3\text{-}TM7}$ but high $RRCS_{TM3\text{-}TM6}$ scores, despite deeper binding modes.

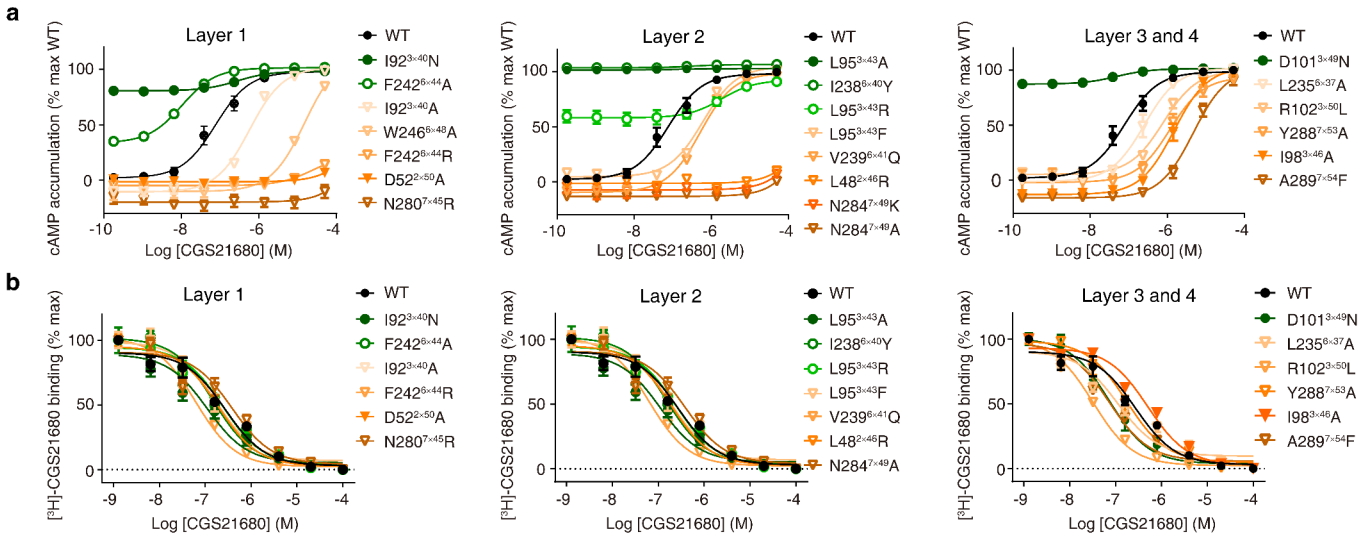

c

Universal activation pathway-guided constitutively activating/inactivating mutations

Layer	Mutation	Expectation based on universal activation pathway			Experimental observation		
		Residue-level effect	Helix-level effect	Expected	Basal activity (% WT)	CGS21680 potency	Binding ability
1	$I92^{3\times40}N$	Form amide-π interaction with $W246^{6\times48}$	Favor the rotation of the cytoplasmic end of TM6, loosen the TM3-6 contacts	Increased G_s engagement	7-fold increase	N.D.	7-fold increase
	$F242^{6\times44}A$	Reduce contacts with $W246^{6\times48}$			2-fold increase	8-fold increase	2.6-fold increase
2	$L95^{3\times43}A(R)$ $I238^{6\times40}Y$	Loosen hydrophobic lock among $L95^{3\times43}$, $I238^{6\times40}$ and $V239^{6\times41}$			28(2)-fold increase	N.D.	3.5(1.4)-fold increase
				cAMP ↑	11-fold increase	N.D.	2-fold increase
4	$D101^{3\times49}N$	Reduce contacts with $R102^{3\times50}$	Favor $R102^{3\times50}$ release		8-fold increase	N.D.	2-fold increase
1	$I92^{3\times40}A$	Reduce contacts with $W246^{6\times48}$	Block the rotation of the cytoplasmic end of TM6, tighten the TM3-6 contacts	Decreased G_s engagement	70.7%	8-fold decrease	1.4-fold decrease
	$F242^{6\times44}R$	Form salt bridge with $D52^{2\times50}$			63.1%	374-fold decrease	2.8-fold decrease
	$W246^{6\times48}A$	Reduce contacts with $I92^{3\times40}$ and $N280^{7\times45}$			80.9%	220-fold decrease	67-fold decrease
	$D52^{2\times50}A$	Destroy hbond network in Na^+ pocket			79.7%	Completely abolished	2-fold increase
	$N280^{7\times45}R$	Form salt bridge with $D52^{2\times50}$	Retard inward movement of TM7 towards TM3, loosen TM3-7 contacts		78.0%	Completely abolished	2-fold decrease
2	$L48^{2\times46}R$	Form salt bridge with $D52^{2\times50}$			93.3%	Completely abolished	1.6-fold increase
	$N284^{7\times49}A$	Destroy hbond network in Na^+ pocket			73.6%	Completely abolished	1.4-fold decrease
	$N284^{7\times49}K$	Form hydrogen bonds with $D52^{2\times50}$ and $N280^{7\times45}$			69.0%	Completely abolished	15-fold decrease
	$L95^{3\times43}F$	Form π-π stacking with $F242^{6\times44}$	Block the rotation of the cytoplasmic end of TM6, tighten the TM3-6 contacts	cAMP ↓	93.2%	8-fold decrease	1.4-fold increase
	$V239^{6\times41}Q$	Form hydrogen bond with $L190^{5\times51}$			80.4%	7-fold decrease	5-fold increase
3	$I98^{3\times46}A$	Reduce contacts with $Y288^{7\times53}$	Retard inward movement of TM7 towards TM3, loosen TM3-7 contacts		71.8%	23-fold decrease	2.5-fold decrease
	$L235^{3\times46}A$	Reduce contacts with $F201^{5\times62}$			71.1%	4-fold decrease	1.5-fold increase
	$Y288^{7\times53}A$	Reduce contacts with residues on TM3			102.6%	16-fold decrease	2-fold increase
	$A289^{7\times54}F$	Clash with $F295^{8\times50}$ upon activation			76.0%	60-fold decrease	4-fold increase
4	$R102^{3\times50}L$	Change physicochemical property	Reduce interaction with G protein		80.0%	10-fold decrease	9-fold increase

Figure 6. Experimental validation of the common activation mechanism. (**a**) cAMP accumulation assay and (**b**) radioligand binding assay: both validated the common activation pathway-guided design of CAMs/CIMs for $A_{2A}R$. Wildtype (WT), CAMs and CIMs are shown in black, green and orange, respectively. (**c**) Mechanistic interpretation of common activation pathway-guided CAMs/CIMs design. N.D.: basal activity was too high to determine an accurate EC_{50} value.

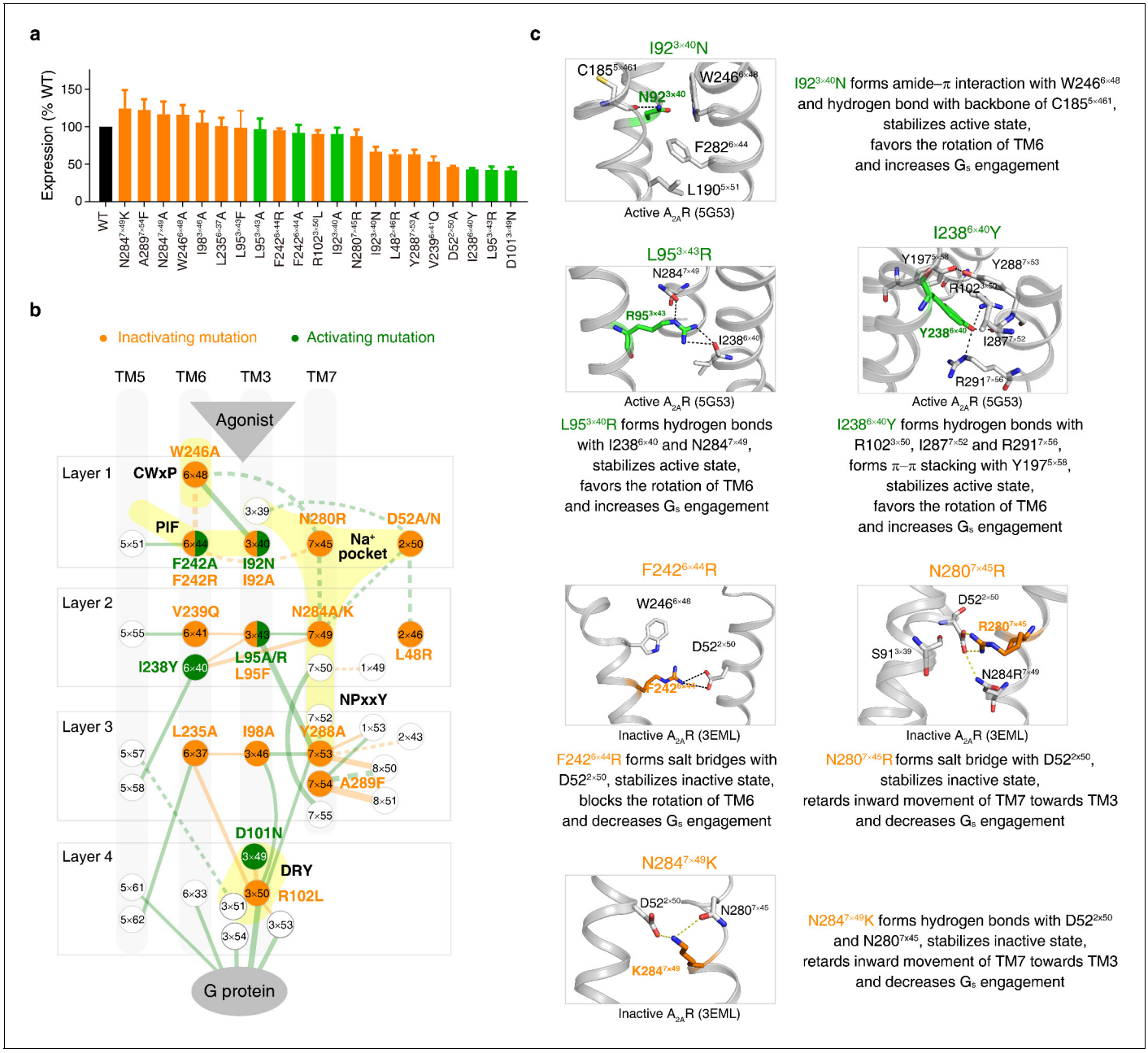

Figure 6—figure supplement 1. Experimental validation of common activation pathway-guided CAM/CIM design for A 2A R. (**a**) Cell surface expression of the WT A $_{2A}$R and its mutants. WT, CAMs and CIMs are colored by black, orange and green, respectively. (**b**) Mapping of validated CAMs/CIMs to the common activation pathway. (**c**) The mechanisms of CAM/CIM design. CAMs and CIMs are in green and orange, respectively.

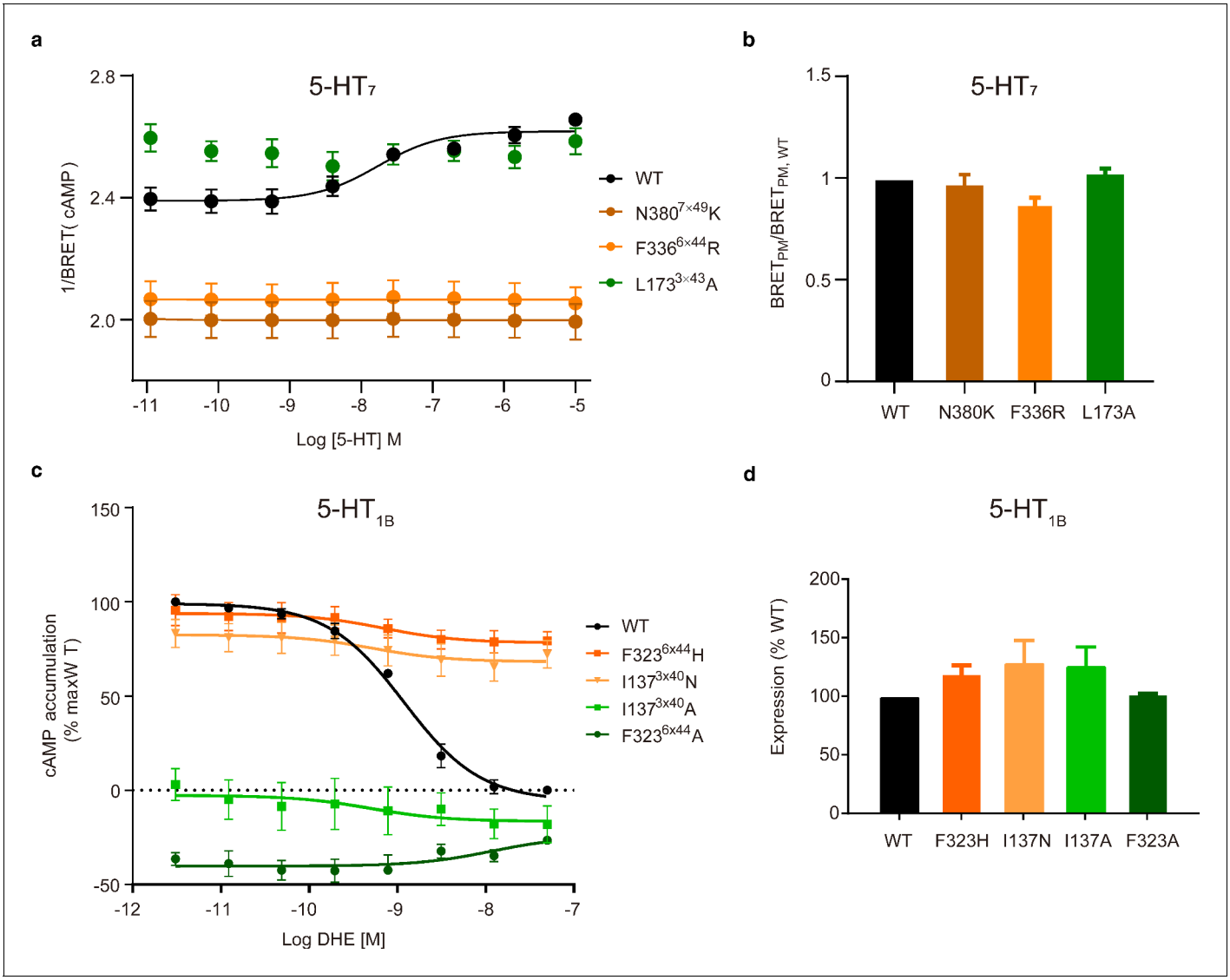

Figure 6—figure supplement 2. Experimental validation of common activation pathway-guided CAM/CIM design for G_s-coupled 5-HT_7 and G_i-coupled 5-HT_{1B} receptors. (**a**) cAMP assay of G_s-coupled 5-HT_7 receptor used an EPAC-based BRET cAMP sensor (n = 6). WT, CAMs and CIMs are colored by black, orange and green, respectively. (**b**) Trafficking assay measured WT and mutant 5-HT_7 receptors in the plasma membrane (PM). (**c**) cAMP measurement of 5-HT_{1B} receptor. CAMs and CIMs are shown in green and orange, respectively. (**d**) Cell surface expression of mutant 5-HT_{1B} receptors relative to that of WT. DHE, dihydroergotamine.

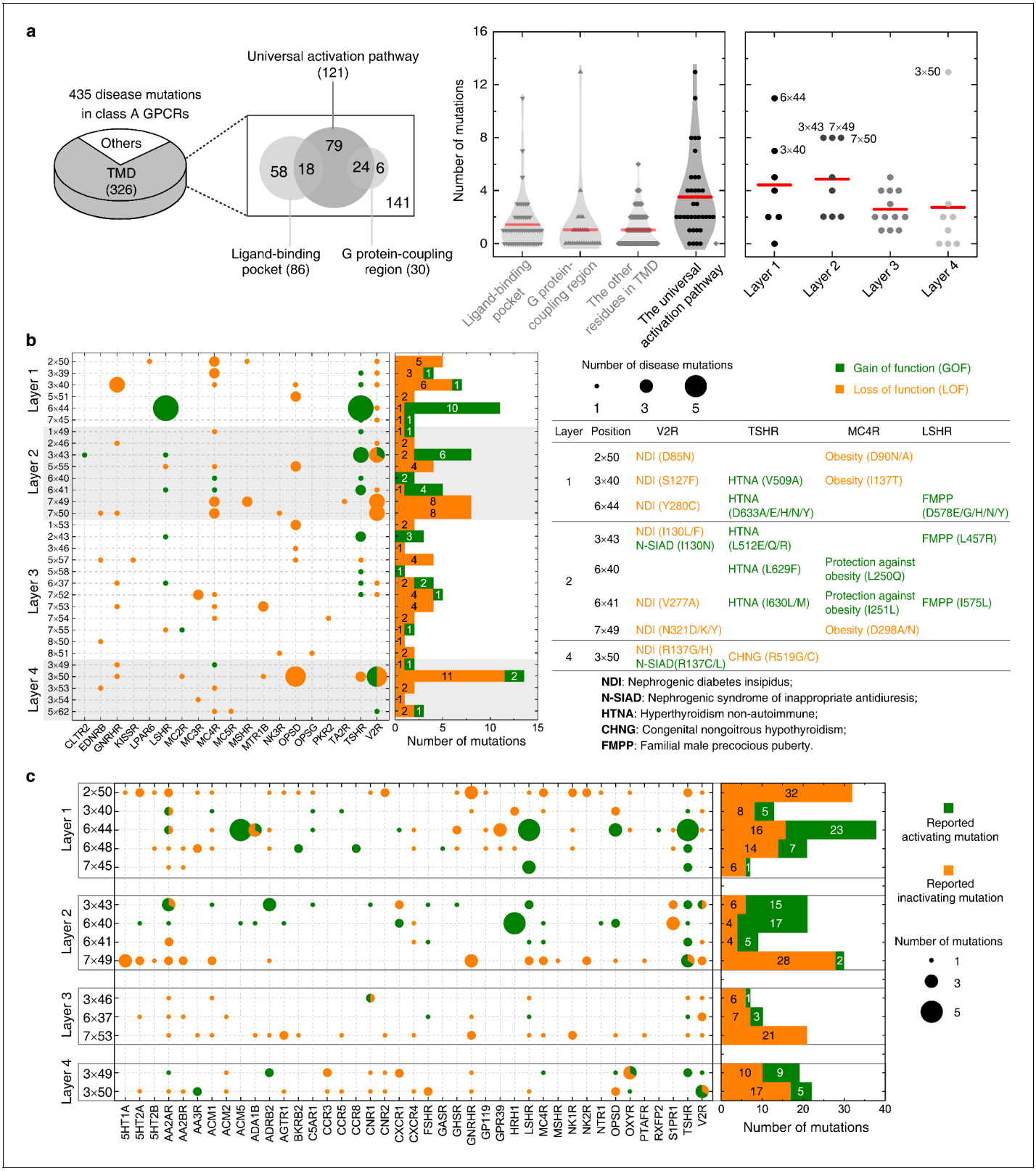

Figure 7. Importance of the common activation pathway in pathophysiological and biological contexts. (**a**) Comparison of disease-associated mutations in the common activation pathway (further decomposed into layers 1–4), ligand-binding pocket, G-protein-coupling region and other regions. Red line denotes the mean value. (**b**) Mapping of disease-associated mutations in class A GPCRs to the common activation pathway. (**c**) Key roles of the residues constituting the common activation pathway have been reported in numerous experimental studies on class A GPCRs. Two hundred seventy two (272) CAMs/CIMs from 41 receptors were mined from the literature for the 14 hub residues (i.e. residues that have more than one edges in the pathway).

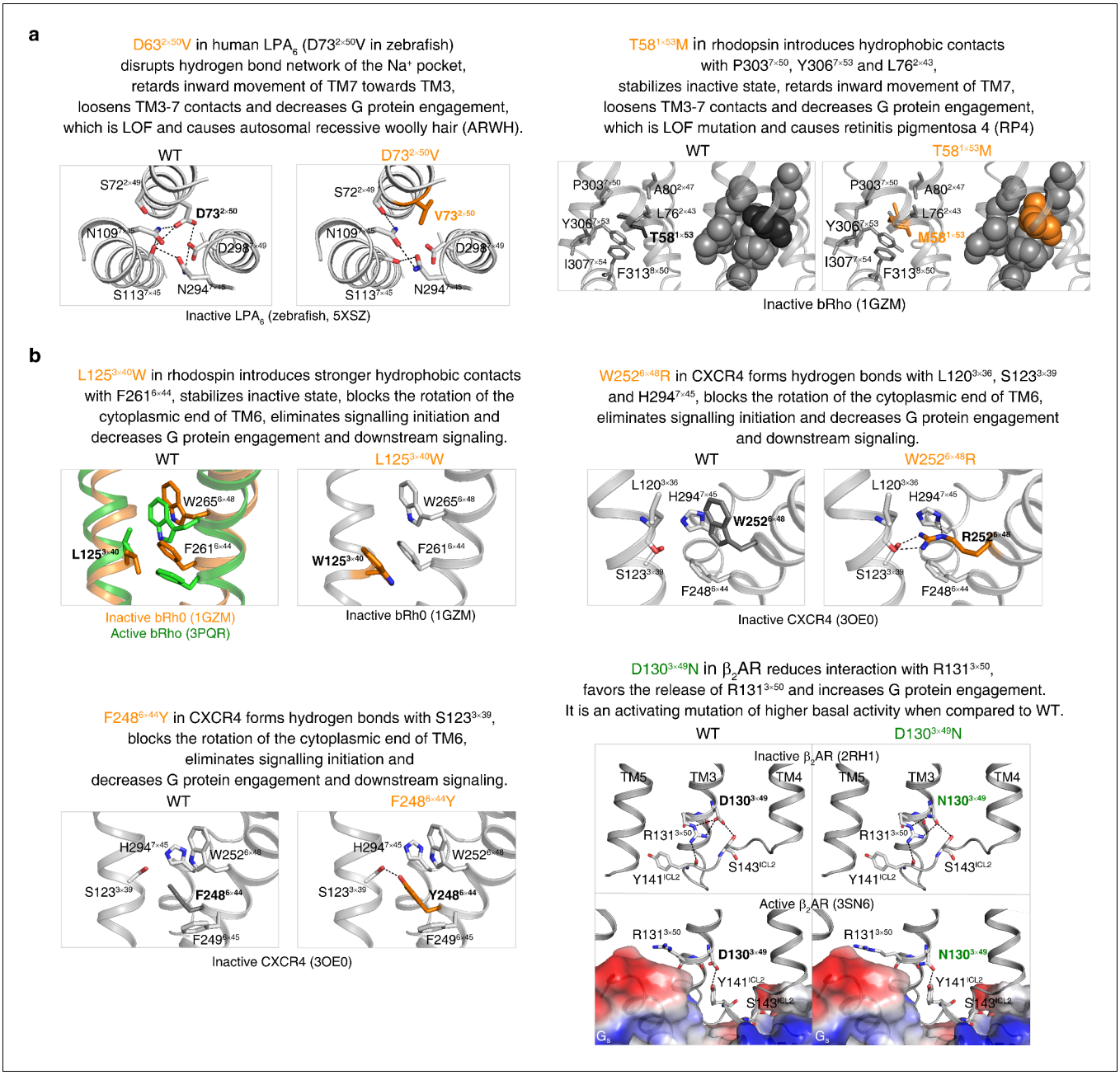

Figure 7—figure supplement 1. The common activation pathway can be used to mechanistically interpret disease-associated mutations and CAMs/CIMs. (**a**) Pathway-guided mechanistic interpretations of two disease mutations. (**b**) Pathway-guided mechanistic interpretations of four CAMs/CIMs.

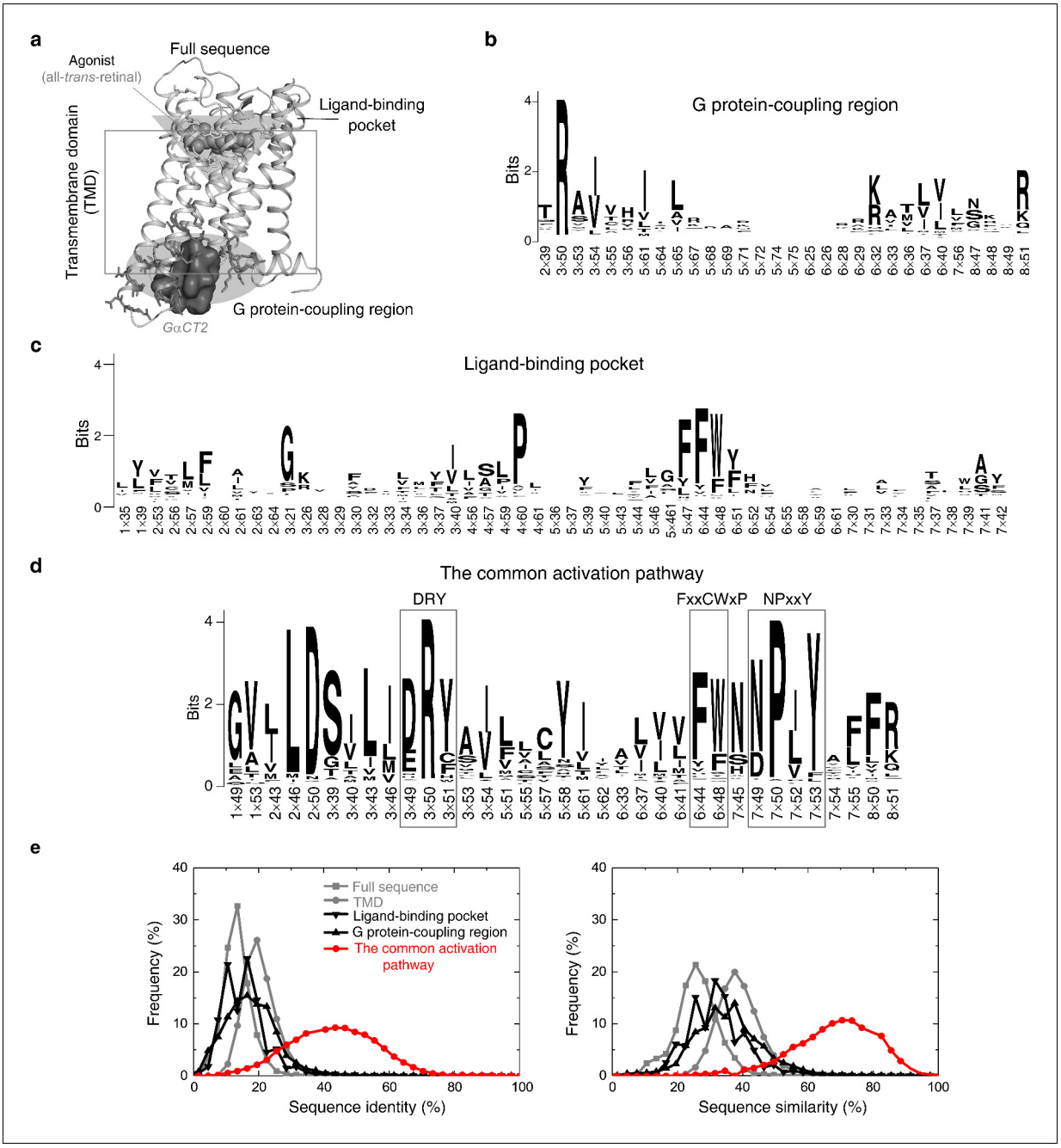

Figure 7—figure supplement 2. Residues in the common activation pathway are more conserved than other functional regions of GPCR. (**a**) Illustration of different functional regions of GPCR. (**b-d**) Sequence pattern of the G protein-coupling region (**b**), ligand-binding pocket (**c**) and the common activation pathway (**d**). (**e**) Distribution of sequence identity (left) and similarity (right) for functional regions across 286 non-olfactory class A receptors.